Presented at the 35th PVSC, June 20-25, 2010, Honolulu, Hawaii

TOWARDS 19% EFFICIENT INDUSTRIAL PERC DEVICES USING SIMULTANEOUS FRONT EMITTER AND REAR SURFACE PASSIVATION BY THERMAL OXIDATION

Sebastian Mack, Ulrich Jäger, Gero Kästner, Edgar Allan Wotke,
Udo Belledin, Andreas Wolf, Ralf Preu, Daniel Biro
Fraunhofer Institute for Solar Energy Systems (ISE),
Heidenhofstr. 2, 79110 Freiburg, Germany

ABSTRACT

Higher solar cell efficiencies enable a reduction of the cost per watt ratio, if production effort is maintained at an acceptable level. A proven high-efficiency concept is the passivated emitter and rear cell (PERC) [1]. However, the transfer of this solar cell structure from demonstrator level to industrial application is challenging. We present a simple approach for the industrial fabrication of PERC solar cells which utilizes the simultaneous passivation of the front emitter and the rear surface by a thin layer of thermally grown oxide. This <u>T</u>hermal <u>O</u>xide <u>P</u>assivated <u>A</u>ll <u>S</u>ides (TOPAS) structure represents an industrially feasible implementation of the PERC concept.

Instead of using masking or sacrificial layers to obtain a structure with a textured, diffused front surface and a plain non-diffused rear surface, side selective wet chemical etching is chosen in this work, since it features a higher cost reduction potential. The current cell design features a selective emitter structure, introduced by laser-doping in combination with conventional screen-printed front contacts.

With the presented approach we achieve an initial efficiency of 18.9 % on large area (149 cm²) 180 µm thick, Czochralski grown, boron doped p-type wafers. The stabilized device reaches a high open circuit voltage of V_{OC} = 641 mV. The comparison of the internal quantum efficiency of the TOPAS device and a full Al-back surface field (BSF) reference reveals a strong advantage in the blue and red response for the TOPAS concept.

INTRODUCTION

Conventional industrial wafer based silicon solar cells feature a homogeneous emitter and a full area aluminum back surface field (Al-BSF). The homogeneous emitter is a trade-off between high lateral conductivity and a low contact resistance on the one side, which would require a low sheet resistance, and an opaque emitter with a low dark saturation current density on the other side, which would require high sheet resistances. By the introduction of a selective emitter structure that features a high dopant density underneath the contacts and a moderate dopant density in between, the blue response of the solar cell is enhanced. Several authors reported an increased efficiency of 0.2-1.4 % (absolute) [2-6] due to the selective emitter structure.

Full area Al-BSF cells have a poor internal rear surface reflectivity and a high surface recombination velocity. Replacing the Al-BSF by a passivated rear surface that is only locally contacted significantly improves the red response and open circuit voltage due to the decreased surface recombination and less parasitic absorption at the rear surface. Although the fill factor decreases due to current crowding at the local contacts, higher efficiencies were demonstrated for such devices [1,7].

The implementation of both a selective emitter and a passivated rear surface (and front, e.g. by a thermal oxide) opens the way to solar cell efficiencies in the 19% range. Nevertheless, the manufacturing process becomes more complex. Until now, expensive masking steps were used often for both front and rear side processing [6]. We circumvent masking steps by using laser-doping for the formation of the selective emitter [4] and single side wet chemical etching [8] for rear side processing for the production of industrial PERC solar cells.

EXPERIMENTAL

Device structure

Figure 1 schematically illustrates the cross capture of the final device, with the dimensions not to scale. The finished device features a selective emitter formed by a laser-doping process, that utilizes the phosphosilicate glass (PSG) as a dopant source [4]. Both front emitter and rear surface are passivated simultaneously by a thin layer of thermally grown oxide. At the front surface, this thin oxide layer is covered by a conventional SiN_X anti-reflection layer, deposited by means of plasma-enhanced chemical vapor deposition (PECVD). A SiO_X PECVD capping layer is deposited onto the oxide layer at the rear surface to enhance the surface passivation and the internal reflectance. Conventional screen-printing of an Ag paste followed by fast-firing in a conveyor-belt furnace forms the front contacts. On the rear surface a laser locally alloys a layer of physical vapor deposited aluminum by means of the laser fired contact (LFC) technology [9]. Thus, the TOPAS structure is a further development of previously published approaches [10], including a selective emitter.

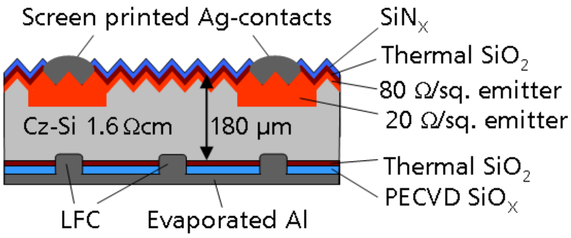

Figure 1 Cross capture scheme of the TOPAS structure.

In the experiment described here, we apply conventional boron-doped Czochralski (Cz) grown wafers with a resistivity of 1.6 Ωcm for the fabrication of TOPAS solar cells. Almost all manufacturing steps are performed using industrial equipment of the PV-TEC pilot line at Fraunhofer ISE [11]. Laboratory equipment is used only for the aluminum deposition, which is performed in an electron beam evaporation system. Note that no edge isolation or other treatment of the wafer edge is required for TOPAS devices.

Emitter characterization

To characterize the TOPAS emitter, we use symmetric samples that feature a diffused emitter on both surfaces. These samples are fabricated from 200 µm thick p-type 1 Ωcm float zone (FZ) wafers using the same processes as for the solar cells, including texturing, emitter diffusion, thermal oxidation, and SiN_X-deposition. No laser doping is applied, thus the samples represent the lowly doped region of the selective emitter structure of the TOPAS device (see Fig. 1). At certain stages of the experiment, we measure the sheet resistance by inductive coupling [12] and the effective carrier lifetime are by quasi-steady-state photoconductance (QSSPC) [13]. The QSSPC technique is used to measure the effective carrier lifetime τ_{eff} at an injection density of Δn = 5*10^{14}cm^{-3}.
The effective surface recombination velocity *S* is calculated according to [14]

$$S = \frac{W}{2}\left[\left(\frac{1}{\tau_{\text{eff}}} - \frac{1}{\tau_{\text{bulk}}}\right)^{-1} - \frac{1}{D}\left(\frac{W}{\pi}\right)^{2}\right]^{-1} \qquad (1)$$

from the sample thickness *W*, the bulk lifetime τ_{bulk} =3 ms (Auger limit) [15], and the diffusion constant *D* = 27.1 cm²/s for the used 1 Ωcm material.
In low-level injection, the emitter dark saturation current density

$$j_{0e} = \frac{qn_i^2}{N_A + \Delta n} S \qquad (2)$$

follows from the intrinsic carrier density n_i = 9.14*10^9 cm^{-3} (at 25°C), the acceptor density N_A and the elementary charge *q*. This recombination current limits the maximum open circuit voltage $V_{oc,max}$ to

$$V_{oc,\max} = V_{th} \ln\left(\frac{j_{sc}}{j_{0e}} + 1\right) \qquad (3)$$

with the thermal voltage V_{th} = 25.7 mV and an assumed short-current density value of j_{sc} = 35 mA cm^{-2}.

RESULTS AND DISCUSSION

Emitter sheet resistance

Table 1 shows the emitter sheet resistance measured by inductive coupling after diffusion and after thermal oxidation. The sheet resistance of the as-diffused emitter is 120 Ω/sq.. The thermal budget of the oxidation process causes a slight drive-in of the emitter, although featuring a much lower thermal budget compared to the drive-in oxidations usually applied for high-efficiency solar cells [1,7]. The additional high temperature step also activates initially inactive phosphorus. Thus, after thermal oxidation we obtain a lowered sheet resistance of 80 Ω/sq.

Processing stage	Sheet resistance
After diffusion	120 Ω/sq.
After oxidation	80 Ω/sq.

Table 1 Emitter sheet resistance R_{sheet} of the lowly doped region of the selective emitter structure after different processing steps measured on reference samples by inductive coupling.

Emitter dark saturation current density

Figure 2 shows the dark saturation current density J_{0e} and the corresponding open circuit voltage limit of the TOPAS emitter at different states of processing. The measurements refer to the emitter region between fingers of the front grid and do not include the highly doped selective area. After the oxidation process, the measurements yield a J_{0e}-value of 260 fA/cm², which limits the open circuit voltage to values below 660 mV. The deposition of a SiN_x layer on both sides of the sample reduces the emitter recombination and leads to a decreased dark saturation current density of 240 fA/cm². Presumably, hydrogen passivation of the emitter bulk and surface reduces the defect recombination in the emitter [16]. Contact firing of the samples seems to release even more hydrogen [16], which further reduces J_{0e} to 160 fA/cm². A final forming gas anneal (FGA) does not change J_{0e} as the SiN_X layer acts as a diffusion barrier for the hydrogen, impeding a further hydrogenation of the Si-SiO_2 interface. Thus, at the end of the cell process, the lowly doped region of the selective emitter features a sheet resistance of 80 Ω/sq. and a J_{0e} of 160 fA/cm² (textured surface), equivalent to 670 mV maximum open circuit voltage.

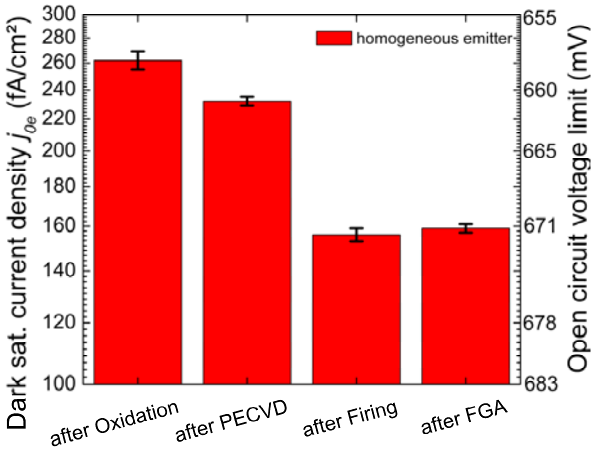

Figure 2 Dark saturation current density and open circuit voltage limit according to Eq. (3) of the TOPAS emitter determined from symmetric lifetime samples. The samples feature a homogeneous emitter with a sheet resistance of 80 Ω/sq. (measured after oxidation). This emitter corresponds to the lowly doped region of the selective emitter structure of the TOPAS cells (see Fig. 1).

Solar cell results

Table 2 shows the parameters from the illuminated current-voltage (IV) curve measured for one group of identically processed cells from the experiment. The data are collected with an industrial cell tester equipped with a flash lamp. The measurement accounts for the spectral mismatch of the TOPAS cells compared to the Al-BSF reference cell. We perform measurements directly after the fabrication process and after illumination for 40 hours at 0.3 suns for fully activating the light induced degradation due to boron-oxygen complex formation [17]. After fabrication, an open-circuit voltage of 645 mV is measured, indicating the high quality of the emitter and rear surface passivation. The superior emitter and rear surface passivation also allows high short circuit current densities of

Device state	V_{oc} (mV)	J_{sc} (mA/cm^2)	*FF* (%)	η (%)
After process				
best cell	645	38.5	76.3	18.9
mean of 6 cells	643	38.4	76.1	18.8
After stabilization				
best cell	641	38.2	75.0	18.4
mean of 6 cells	638	38.0	74.9	18.2

Table 2 Solar cell parameters for one group of identically processed cells of the experiment. Cell area is 149 cm². The cell tester measurement accounts for the spectral mismatch of the TOPAS cells compared to the Al-BSF reference cell. Measurements are performed directly after the fabrication process and after stabilization by 40 hours illumination at 0.3 suns.

38.5 mA/cm². The achieved efficiency of 18.9 % demonstrates the potential of our TOPAS approach. The mean efficiency of six equally processed solar cells is 18.8 %. Light-induced degradation reduces the efficiency to 18.4 % for the best cell.

Quantum efficiency analysis

Figure 3 shows the global (full area) internal quantum efficiency (IQE) of a TOPAS solar cell and two Al-BSF cells, one with a homogeneous emitter and the other with a selective emitter. The selective emitter of the Al-BSF cell is produced by laser-doping as well, however, in contrast to the TOPAS cells, the emitters of the Al-BSF cells do neither receive wet chemical cleaning nor thermal oxidation. All cells are stabilized before the measurement.
The TOPAS cell exhibits a higher IQE than the other two cell concepts for both short and long wavelength region. In the short wavelength region, the TOPAS emitter benefits from the surface removal during wet chemical cleaning and the subsequent oxidation which yields an improved surface passivation. The IQE therefore also exceeds that of the selective emitter cell, which already shows a superior IQE compared to a homogeneous emitter. The TOPAS device reaches a very high IQE-value of 96 % at a wavelength of 400 nm.

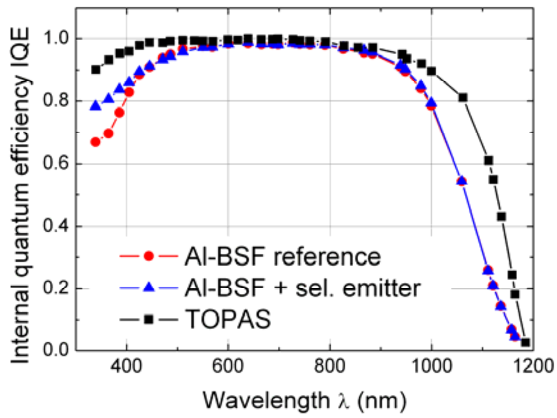

Figure 3 Global, differential internal quantum efficiency of a TOPAS cell and two Al-BSF references, one with a homogeneous emitter and one with a selective emitter. The IQE measurement is performed at a bias illumination level of 0.1 suns. All cells are stabilized by at least 36 hours illumination at 0.3 suns before the measurement.

The impact of the passivated rear surface is visible in the long wavelength region. Due to the thermal oxide passivation and only locally defined contacts, the effective surface recombination velocity is drastically decreased, compared to a conventional full area Al-BSF. Furthermore, the thermal oxide in combination with the deposited dielectric capping layer acts a dielectric mirror with a high internal reflectance. Long wavelength photons are more likely reflected back into the bulk, increasing the probability of carrier generation. At a wavelength of 1000 nm, an IQE value of

90 % is found for the TOPAS cell concept, whereas the standard Al-BSF cells feature values of less than 80 %. A quantitative analysis of the IQE [18] yields an effective diffusion length of 720 µm for the TOPAS cell, corresponding to more than 4 times the cell thickness, and 420 µm for the Al-BSF devices. The increased effective diffusion length of the TOPAS cell confirms the superior rear surface passivation compared to the Al-BSF technology.

Rear surface planarization

Figure 4 illustrates the influence of different single sided wet chemical polishing steps on the open-circuit voltage V_{OC} and the short-circuit current density J_{SC} of TOPAS cells. Gravimetric measurements yield the average amount of silicon removed by the different etching processes. If no polishing step is performed, the mean open-circuit voltage is 620 mV. Increasing the amount of silicon removed by the etching process yields higher open-circuit voltages. A similar trend is observed for the short-circuit current density. The polishing step levels the rear surface by removing the random pyramids, leading to a more homogeneous surface and higher open-circuit voltages. This result is consistent with previously published data [8]. When removing ~15 µm of silicon a high mean V_{OC} of 643 mV is obtained. This corresponds to an increase of over 20 mV compared to the samples processed without a polishing step. The mean J_{SC} increases from 36.9 mA/cm² to 38.2 mA/cm². Simulations show that a gain in V_{OC} of less than 0.2 mV is expected from the 15 µm lower device thickness alone. Thus not the device thickness but the rear surface morphology shows a large impact on V_{OC}.

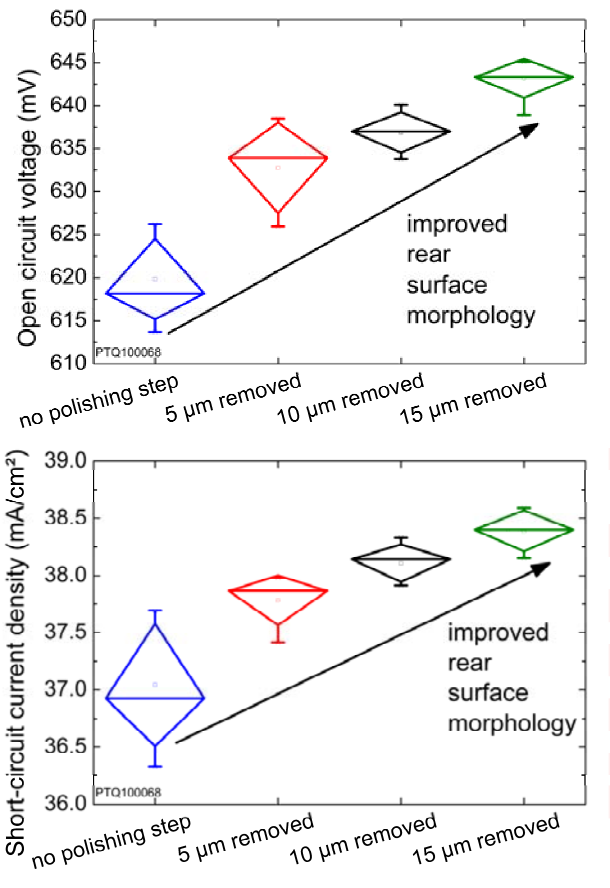

Figure 4 Influence of different rear surface polishing steps on the open-circuit voltage (top) and short-circuit current density (bottom) of TOPAS solar cells. Shown are minimum, maximum, average (dot), and median (hor. line) value, as well as standard deviation (diamonds) for groups of 3 to 6 identically processed cells. The cells were not stabilized before the IV-measurement.

Figure 5 shows confocal microscope topographies before and after a single side wet chemical polishing step, with both pictures of the same scale. As the random pyramids on the left hand side are of different size and height, they form a very uneven surface. The picture on the right hand side of Figure 5 shows a surface after a polishing step. Gravimetric measurements indicate a reduced wafer thickness of 15 µm due to the polishing step. The height distribution on the surface is now more homogeneous. Nevertheless, even after removing 15 µm of silicon, residuals of the random pyramid texture are still visible. Therefore, it is possible that a smoother surface would allow even higher V_{OC} and J_{SC} values.

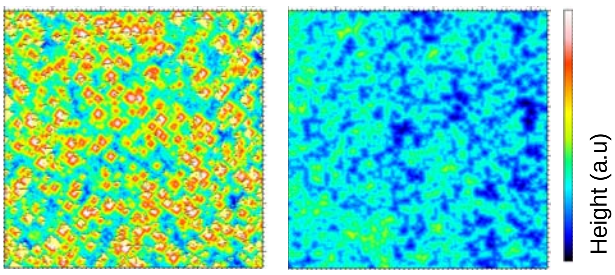

Figure 5 Confocal microscope topography of a textured surface before (left) and after (right) the single sided wet chemical polishing process. The images are equally scaled. Here, ~15 µm of silicon are removed by the polishing step.

SUMMARY

In this paper, we present a new approach for the industrial production of screen-printed PERC solar cells. The Thermal Oxide Passivated All Sides (TOPAS) cell process circumvents costly masking steps, using laser-doping for the selective emitter formation and inline side selective wet chemical etching for rear surface processing. The growth of a thin thermal oxide simultaneously passivates both emitter and rear surface. The TOPAS emitter (lightly doped region) features a sheet resistance of 80 Ω/sq. and a dark saturation current density of 160 fA/cm² for a textured surface.

With the TOPAS approach, high efficiencies of up to 18.9 % (not stabilized, unconfirmed) are achieved for a 180 µm thick device fabricated from conventional boron-doped Cz material. An analysis of the internal quantum efficiency shows a strong increase in both the blue and red

response for the TOPAS cell compared to a conventional Al-BSF cell, confirming the superior emitter and rear surface passivation of the TOPAS device.
The parameters for the single sided wet chemical etching process are crucial for the performance of TOPAS cells. Both V_{OC} and J_{SC} strongly increase with the amount of silicon removed during etching. Apparently, the smoother surface morphology reduces the recombination at the rear surface. Thus, smoother surfaces than those realized in this work could further improve the device performance.

Acknowledgments

We gratefully acknowledge the technical support by the PV-TEC coworkers. This work is supported by the German Federal Ministry of Environment, Nature Conservation and Nuclear Safety under contract 0329849B. Further support by the EU funded project “ULTIMATE” under the project number ENERGY-2007-2.1-09 is gratefully acknowledged.

REFERENCES

[1] A. W. Blakers et al., "22.8% efficient silicon solar cell", *Appl. Phys. Lett.* **55**, 1989, pp. 1363-1365.

[2] F. Book, B. Raabe, and G. Hahn, "Two diffusion step selective emitter: comparison of mask opening by laser or etching paste", *Proceedings of the 23rd European Photovoltaic Solar Energy Conference*, 2008, pp. 1546-1549.

[3] A. Dastgheib-Shirazi et al., "Selective emitter for industrial solar cell production: a wet chemical approach using a single side diffusion process", *Proceedings of the 23rd European Photovoltaic Solar Energy Conference*, 2008, pp. 1197-1199.

[4] U. Jäger et al., "Selective emitter by laser doping from phosphosilicate glass", *Proceedings of the 24th European Photovoltaic Solar Energy Conference*, 2009, pp. 1740-1743.

[5] T. Lauermann et al., "INSECT: An inline selective emitter concept with high efficiencies at competitive process costs improved with inkjet masking technology", *Proceedings of the 24th European Photovoltaic Solar Energy Conference*, 2009, pp. 1767-1770.

[6] M. Weiß et al., "Selective emitter from structured diffusion source proves its capability in industrial realization", *Proceedings of the 24th European Photovoltaic Solar Energy Conference*, 2009, pp. 1941-1944.

[7] A. G. Aberle et al., "High Efficiency Silicon Solar Cells: Si/SiO_2 Interface Parameters and their Impact on Device Performance", *Prog. Photovolt: Res. Appl.* **2**, 1994, pp. 265-273.

[8] J. Rentsch et al., "Single side etching - key technology for industrial high efficiency processing", *Proceedings of the 23rd European Photovoltaic Solar Energy Conference*, 2008, pp. 1889-1892.

[9] E. Schneiderlöchner et al., "Laser-fired contacts (LFC)", *Proceedings of the 17th European Photovoltaic Solar Energy Conference*, 2001, pp. 1303-1306.

[10] J. Rentsch et al., "Technology route towards industrial application of rear passivated silicon solar cells", *4th World Conference on Photovoltaic Energy Conversion*, 2006, pp. 1008-1011.

[11] D. Biro et al., "PV-Tec: retrospection to the three years of operation of a production oriented research platform", *Proceedings of the 24th European Photovoltaic Solar Energy Conference*, 2009, pp. 1901-1905.

[12] M. Spitz, U. Belledin, and S. Rein, "Fast inductive inline measurement of the emitter sheet resistance in industrial solar cell fabrication", *Proceedings of the 22nd European Photovoltaic Solar Energy Conference*, 2007, pp. 47-50.

[13] R. A. Sinton, A. Cuevas, and M. Stuckings, "Quasi-steady-state photoconductance, a new method for solar cell material and device characterization", *Proceedings of the 25th IEEE Photovoltaic Specialists Conference*, 1996, pp. 457-460.

[14] A. B. Sproul, "Dimensionless solution of the equation describing the effect of surface recombination on carrier decay in semiconductors", *J. Appl. Phys.* **76**, 1994, pp. 2851-2854.

[15] M. J. Kerr and A. Cuevas, "General parameterization of Auger recombination in crystalline silicon", *J. Appl. Phys.* **91**, 2002, pp. 2473-2480.

[16] H. F. W. Dekkers and G. Beaucarne, "Molecular hydrogen formation in hydrogenated silicon nitride", *Appl. Phys. Lett.* **89**, 2006, pp. 1-3.

[17] J. Schmidt and K. Bothe, "Structure and transformation of the metastable boron- and oxygen-related defect center in crystalline silicon", *Phys. Rev. B* **69**, 2004, pp. 0241071-0241078.

[18] B. Fischer et al., "Scanning IQE-measurement for accurate current determination on very large area solar cells", *Proceedings of the 29th IEEE Photovoltaics Specialists Conference*, 2002, pp. 454-457.